Macalester Journal of Physics and Astronomy

May 2015

Modelling Transient Terahertz Magneto-Spectroscopy measurements of p-type CVD Graphene leading to a negative photoconductivity.

Rhyan Foo Kune
Macalester College, rfookune@macalester.edu

Abstract

Ultrafast Terahertz (THz) Magneto-Spectroscopy (UTMS) measurements were performed on p-type CVD graphene sample to investigate the intrinsic carrier dynamics of the material. We investigated static and time-resolved THz transmission measurements, in which the sample was photo-excited by a near infrared (NIR) pump pulse, in order to study its behavior in a magnetic field. In these measurements the free carriers were probed to independently measure the carrier density and scattering rate in this film. We observed, in our graphene sample, an increase in transmission related to a negative photoconductivity (decrease in conductivity after photoexcitation) consistent with previous research. This decrease is predicted by our model and relate to the energy dependence of the scattering process considered in this paper.

Follow this and additional works at: http://digitalcommons.macalester.edu/mjpa

Part of the Atomic, Molecular and Optical Physics Commons, and the Condensed Matter Physics Commons

MACALESTER COLLEGE

Modelling Transient Terahertz Magneto-Spectroscopy measurements of p-type CVD Graphene leading to a negative photoconductivity.

Rhyan F. Y. Foo Kune & Prof. J. N. Heyman

Macalester College

2015

Abstract

Ultrafast Terahertz (THz) Magneto-Spectroscopy (UTMS) measurements were performed on p-type CVD graphene sample to investigate the intrinsic carrier dynamics of the material. We investigated static and time-resolved THz transmission measurements, in which the sample was photo-excited by a near infrared (NIR) pump pulse, in order to study its behavior in a magnetic field. In these measurements the free carriers were probed to independently measure the carrier density and scattering rate in this film. We observed, in our graphene sample, an increase in transmission related to a negative photoconductivity (decrease in conductivity after photoexcitation) consistent with previous research. This decrease is predicted by our model and relate to the energy dependence of the scattering process considered in this paper.

I.   Introduction

Graphene is a single-atom thick layer of carbon arranged in a honeycomb lattice (Figure 1) with a gapless band structure. Graphene has linear energy dispersion describing "Dirac cones" around the Brillouin zone. At this point the valence and conduction band crosses (Figure 2). This allows carrier to move easily between the two bands, making it a great conductor of heat and electricity. Furthermore, this stable 2D material has carriers with zero effective mass and exhibits high mechanical strength and flexibility. All those properties displayed by graphene make it a promising candidate for future electronic devices. Andre Geim and Konstantin Novoselov were awarded the 2010 Nobel Prize in Physics for the groundbreaking discovery of this material. Understanding the dynamics of carriers within this material and their response to optical excitation is fundamental to determine the viability for large-scale manufacturing purposes and other feasible applications.

Ultrafast THz spectroscopy measurements have been extensively used to probe the intrinsic properties of graphene [1] [2] [3]. This technique, explained in more detailed in the latter section of this paper, serves as a contactless electrical probe to observe phenomenon happening on a sub-picosecond time scale. Previous transient studies of hot carrier dynamics in graphene reveal that the THz spectrum, before and after photoexcitation, exhibits a simple Drude response [4] [5] [6]. Two distinct behaviors have been observed for the transient conductivity in graphene. Some studies show an increase of THz transmission in single-layer CVD graphene leading to a decrease in conductivity due to photoexcitation. Other report a decrease in THz transmission in epitaxial multilayer graphene on SiC. Shi *et. al.* [5] argue that these seemingly contradictory results are linked to the doping of the samples. Charge neutral point graphene exhibits positive photoconductivity, whereas highly doped graphene samples show a decrease in conductivity [5].

In this study, an optical pump-terahertz probe measurement was used to report the transmission of *p*-type CVD graphene in a magnetic field to terahertz radiation. Complex conductivity in CVD graphene

Rhyan Foo Kune & James Heyman   3

and its response to photo-excitation was deduced from the THz transparency of the material. These set of measurements allows us to independently extrapolate the carrier concentration and carrier mobility of our samples. In such a material a, the conductivity tensor, resulting from an applied magnetic field, is given by

$$\begin{pmatrix} \sigma_{xx} & \sigma_{xy} \\ \sigma_{yx} & \sigma_{yy} \end{pmatrix} = \frac{\sigma_0}{1 + \omega_c^2 \tau^2} \begin{pmatrix} 1 & \omega_c \tau \\ -\omega_c \tau & 1 \end{pmatrix} \quad [7]$$

where σ_0 is the zero-field conductivity, ω_c is the cyclotron frequency and τ the scattering rate. The subscripts xx, xy, yx and yy relates to the different component of the conductivity related to the motion of free carriers in a magnetic field. We observe that that the ratio of σ_{xx} over σ_{xy} is proportional to the magnetic field and determines the carrier mobility.

$$\frac{\sigma_{xy}}{\sigma_{xx}} = \omega_c \tau = \mu B$$

Assuming a Drude like model, we can determined the carrier density from the mobility as

$$\sigma_{Drude} = ne\mu$$

where σ_{Drude} reflects the conductivity, e is the electron charge and n the carrier density. The same Drude-like behavior was assumed by Hwang *et. al* [4].

A model was further developed to characterize the behavior observed. The model to our experimental data was derived from proposed theories on carrier-phonon dynamics and recombination rates in graphene.

II.   Theory

In order to characterize our terahertz magneto spectroscopy measurements, we adapted a model of transient photoconductivity in graphene proposed by Rana, *et. al* [8] [9]. This model assumes that the photoexited electrons thermalize on a time scale of ~ 10fs which is below the resolution of our experiment. This allows us to define a single electron temperature [6]. The hot carriers cool as a result of phonon-

scattering and the model determines the carrier temperature (T_e), electrons and holes densities, and scattering rates, as well as the conductivity as a function of time.

In order to define those parameters, the following procedure was utilized. The background doping and the photoexcitation of carriers by the laser pump pulse gives an initial thermal energy (Q_0) to the system which starts with an initial hole density (N_0). We assume that hot carriers, resulting from the transient pump pulse, thermalize on a shorter time scale than our experimental resolution. This allows us to translate the thermal energy into a single carrier temperature (T_e). Assuming a distribution function dependent on a single carrier temperature and chemical potential, we define the population of electrons ($n_e(E)$) and holes ($n_h(E)$) as a function of energy. A similar thermal distribution assumption was made by Hwang *et. al* [4]. The Fermi-Dirac distribution function is given by

$$f(\epsilon) = \frac{1}{e^{(\epsilon - \mu)/kT} + 1}$$

where ϵ is the energy, μ the chemical potential, k boltzman's constant and T the carrier temperature. The appropriate distribution function was found by modulating the chemical potential to fit our data and knowing the initial carrier density.

Previous studies report a two-step cooling process in graphene [1]. A fast relaxation due to carrier-carrier scattering followed by a slow relaxation rate due to carrier-phonon scattering. The fast cooling process cannot, however, be observed in our measurements due to the resolution of measurement, as stated above. Therefore, we assumed that the main factor in our scattering process was due to the interaction with phonons. We assume that only two types of phonon dominate the scattering process. K-phonons describe the intervalley scattering, while Γ-phonons relate to intravalley scattering.

For an electron at a given thermal energy (E), the scattering rate for optical phonon emission (G) and absorption (R) are given by [8] [9]

$$R(E) = 2OA\left[\frac{E - E_p}{E_p}\right]\left(1 - f(E - E_p)\right)(1 + N)$$

Rhyan Foo Kune & James Heyman

$$G(E) = 2A \left[\frac{E + E_p}{E_p} \right] (1 - f_2(E + E_p))N$$

Here, E_p is the phonon energy, f and f_2 are distribution functions for the initial and final energy states, N is the phonon density and $A = \frac{9}{4} \left(\frac{\partial t}{\partial b} \right)^2 \frac{\hbar \omega}{\pi \rho \omega \hbar^4 v^4}$. O is a parameter that controls the sign of the expression, ensuring that the energy difference remains positive for both interband ($E < E_p$) and intraband ($E > E_p$) transitions.

The phonon emission and absorption rates were evaluated for a range of electron and hole energy states for phonon scattering. We then integrated over the considered energy states to find the total phonon emission and absorption rates, which specify the average carrier scattering rate (τ) due to phonon interaction. In addition to phonon scattering, an adjustable background scattering rate was included to account for scattering due to impurity and defects in the sample. This background scattering is assumed to be temperature independent. The scattering rates in graphene define the cooling rate for the hot carriers at a particular carrier temperature. The change in temperature dT_e correlates with the decrease in energy in the electron gas and can be expressed in terms of electron-hole recombination and generation rates. [8] [9]

$$\frac{dT_e}{dt} = \frac{(n\langle R_{\Gamma e} \rangle + p\langle R_{\Gamma h} \rangle)\hbar \omega_\Gamma + (n\langle R_{Ke} \rangle + p\langle R_{Kh} \rangle)\hbar \omega_K}{C_e + C_h}$$

The rate of change in the optical phonon populations is given by the absorption and emission rates

$$\frac{dn_\Gamma}{dt} = \left(\frac{nR_{\Gamma e} + pR_{\Gamma h}}{M_\Gamma} \right) - \frac{n_\Gamma - n_\Gamma^0}{T_{ph}}$$

$$\frac{dn_K}{dt} = \left(\frac{nR_{Ke} + pR_{Kh}}{M_K} \right) - \frac{n_K - n_K^0}{T_{ph}}$$

n_Γ and n_K are the phonon population, n_Γ^0 and n_K^0 are the phonon densities at equilibrium (300 K), n is the electron density and p the density of holes. C_e and C_h are the electron and hole heat capacities. M_Γ and M_K are defined as the number of phonon modes around the Γ-point and K-point.

Starting with the initial carrier temperature and phonon density, these equations are stepped forward in time to calculate the change in carrier temperature, carrier density and phonon density. The procedure is

Rhyan Foo Kune & James Heyman

then repeated for the next time increment using the new carrier temperature and phonon densities. The time dependent conductivity was computed from those parameters. Figure 3 provides a schema of the model described above.

III.   Experiment

The synthesis of our graphene on sapphire samples was done through chemical vapor deposition (CVD) following Li *et. al.* .[10] In this process, a copper substrate is heated in a low vacuum furnace and a mixture of hydrogen and methane gas is injected into the chamber. Hydrogen causes the methane and metal to react, depositing a carbon atom onto the Cu substrate. The metal is removed using an etchant solution and the graphene obtained is then transferred onto a sapphire substrate and the polymer is dissolved. Our CVD graphene samples were produced and distributed by Dr. Jeremy Robinson from the Naval Research Laboratory in Washington DC. Figure 4 illustrates the procedure used to produce our chemical vapor deposition (CVD) graphene samples.

A THz frequency light pulse interacts mostly with free electrons as it passes through a material. Looking at the percent of terahertz transmission through a sample allows us to determine the carrier dynamics in graphene. Specifically probing the change in orientation of transmitted THz radiation after going through a sample, we can also determine the motion of the free electron in the system. The elements of the conductivity tensor can be determined from the polarized transmission using standard thin film approximation. For $\alpha = \frac{\mu_0 c}{n+1}$ where μ_0 is the vacuum permeability constant, c the speed of light and n the index of refraction of the reference:

$$\sigma_{xx} = \left[\frac{1}{t_{xx}} - 1 \right] * \left(\frac{1}{\alpha} \right)$$

$$\sigma_{xy} = \left[\frac{t_{xy}}{(t_{xx})^2} \right] * \left(\frac{1}{\alpha} \right)$$

Rhyan Foo Kune & James Heyman

7

The two component of the conductivity tensor needed to define the carrier mobility and carrier density can therefore be recorded through THz transmission measurements.

THz transmission measurements were performed on samples in a magnetic field. Our samples were photoexcited by a femtosecond pump pulse and probed using THz signal. Our THz system includes a Ti:Sapphire chirped pulse oscillator emitting 0.5µJ, 50 fs laser pulses at wavelength 800 nm and a repetition rate of 5 MHz. A photoconductive switch served to generate horizontally polarized pulses of THz radiation. The sample was mounted in a Magneto-Optical Cryostat and was surrounded by a helium gas ambient at 240K. This superconductive magnet allows us to maintain the sample in at a constant magnetic field. The THz field was probed using a 1mm-thick ZnTe crystal as an electro-optic detector. The detector allows us to record the propagating electro-magnetic pulses through the Pockels effect as the refractive index of the ZnTe detector changes with the intensity of the THz field [11]. The path of the THz pulses was purged with dry air to prevent THz absorption by water vapor. Wire-grid polarizers were placed before and after the sample. The first polarizer was set to pass horizontally polarized radiation, and the second polarizer as well as the electro-optic detector could be rotated to detect either the horizontally or vertically polarized components of the transmitted radiation. These set of polarizers allows us to define precisely the orientation of the THz light before and after interacting with our sample. The experimental setup is described in Figure 5. Figure 6 illustrate the expected behavior of the THz signal for our pump-induced photoexcitation THz measurement.

For linear transmission measurements, we probed the time dependent-electric field of THz pulses transmitted through the samples and through a reference sample. We recorded the horizontally polarized component transmitted through the sample and through the reference ($S_{xx}(t)$ and $R_{XX}(t)$ respectively) as well as the vertical component transmitted through the sample ($S_{xy}(t)$). The Fourier Transform of each waveform yields the corresponding single beam spectrum (amplitude and phase). The complex transmission is the ratio of sample and reference spectra. We define $t_{xx} = S_{xx}(f)/R_{xx}(f)$ and $t_{xy} = S_{xy}(f)/R_{xx}(f)$. The THz conductivity of the sample at equilibrium was monitored continuously over a

range of magnetic fields. During those magnetic sweeps, multiple THz conductivity measurements were recorded repeatedly while ramping up the magnet system to higher fields. For each of those measurements, the signal was probed at the same point on the waveform which we chose as the peak value of the transmission recorded without the presence of a magnetic field.

This novel experimental procedure was applied to a well-characterized test sample consisting of an *n*-type GaAs epitaxial layer grown on a silicon substrate. GaAs sample shows complex behavior of conductivity with magnetic field. σ_{xx} describes a parabola while σ_{xy} describes a curved line with negative rate of change. As expected, we see a linear relation with magnetic field for the ratio σ_{xy}/σ_{xx}. The slope of the line gives the mobility of free carriers in the sample. Reported experimental results for carrier mobility and density, derived from the Drude model, gave reasonable agreement with the predicted values (Figure 7).

Time-Resolved THz Magneto-Spectroscopy measurements were carried on the sample. In these measurements the sample is photoexcited with a femtosecond pump pulse and the change in THz transmission is measured as a function of delay time between the pump pulse and the THz probe pulse. A chopper was used to modulate the pump beam, and the change in signal was monitored with a lock-in amplifier. As reported in several studies, the transmission of CVD graphene is not strongly frequency dependent over the THz spectral range [6]. The weak dependency of our sample to frequency allows us to monitor changes in transmission by tracking the change in amplitude of a single point in the THz waveform which we chose to be the peak of the amplitude.

The change in the THz electric field, due to the pulse traversing the sample, was recorded in both the horizontal and vertical polarization ($\delta_{xx}(t)$ and $\delta_{xy}(t)$ respectively). We define $dt_{xx} = \delta_{xx}(f) / R_{xx}(f)$ and $dt_{xy} = \delta_{xy}(f) / R_{xx}(f)$. The change in conductivity was derived from the expressions for σ_{xx} and σ_{xy} defined above

$$d\sigma_{xx} = -\frac{1}{\alpha t_{xx}^2} dt_{xx}$$

$$d\sigma_{xy} = \frac{1}{\alpha t_{xx}^2} dt_{xy}$$

Rhyan Foo Kune & James Heyman

9

Time-Resolved sweep measurements were performed by monitoring the change in the signal throughout a range of magnetic fields.

IV.   Results

Linear Time-Domain THz magneto-spectroscopy measurements of graphene on a sapphire substrate are shown in Figure 8 a) (σ_{xx} vs. *B* and σ_{xy} vs. *B*). The σ_{xx} signal decreases as we move away from zero magnetic field, describing a nearly symmetric figure. A σ_{xy} component to the net conductivity also appears with an antisymmetric behavior observed around the origin with a positive rate of change at every point. σ_{xy} becomes tangential at high magnetic field. The changes in σ_{xx} and σ_{xy} away from the origin are small.

Those behaviors are similar to those seen in our GaAs sample. However, the tangential slope of σ_{xy} at every point changes in sign. We observe an increase in σ_{xy} for our graphene sample whereas our GaAs samples exhibit a decrease in σ_{xy}. The discrepancy can be explained through the doping level of each sample. While our CVD graphene sample is *p*-type (excess of holes), our GaAs sample is *n*-type (excess of electron).

Figure 8 b) shows the ratio σ_{xy}/σ_{xx} versus magnetic field. As expected, while the behavior of each component is complex with magnetic field, their ratio is approximately linear with magnetic field. The slope of the graph gives the mobility of carriers in the sample.

The model developed in the section above gives a fit describing a mobility of $\mu = 0.18 \ m^2/V.s$. We obtain a carrier concentration $p = 2.0 \cdot 10^{12} \text{cm}^{-2}$ and average scattering time $\tau = 37$fs. We observe a significant discrepancy (~50%) between these values recorded in a helium gas at 240K and those obtained from FTIR measurements taken at room temperature in air. FTIR is a reliable technique extensively used in solid state physics. This approach has already been used to study the exotic properties of graphene. The reported discrepancy may reflect the strong environmental sensitivity observed in graphene [12].

A time-resolved version of the same measurements is shown in Figure 9 a). This figure records the peak conductivity change due to photoexcitation versus magnetic field. We observe a change in conductivity of the order of 5% in our graphene films after photoexcitation ($\varphi = 3.17*10^{-8}$ *W/cm*). We see a negative photoconductivity of σ_{xx}. $\Delta\sigma_{xx}$ is nearly symmetric with magnetic field while $\Delta\sigma_{xy,}$ on the other hand, is antisymmetric with magnetic field.

Figure 9 b) shows the fit to the time-resolved measurements using the model developed above. Using three adjustable parameters, the initial input thermal energy from photoexcitation, the single chemical potential and the background scattering rate due to impurity, we observed a good correlation between the model and the data set.

V.   Discussion

The Time-Domain magneto-spectroscopy data (without photoexcitation) gave values for both carrier density ($n=2.7*10^{12}$ cm^{-2}) and mobility ($\mu=0.18$ cm^2/(V.s)). Although the overall behavior of the conductivity seems to be consistent with our expectation, we observed a high discrepancy with the values predicted by FTIR measurements. This discrepancy can be explained through the high sensitivity of graphene to the environment. While FTIR measurements were carried in an air atmosphere at 300K, our measurements were done in a helium gas at 240K due to the restriction imposed by conducting our experiment with a superconductive magnet.

The model, derived from Rana, *et al.* [8] [9], as described previously offers an approximation to our Time Resolved experimental measurements. Negative photoconductivity was observed in our graphene samples. Assuming a Drude-like response, our result confirms previous measurements done on single layer CVD graphene. This behavior has been observed in highly doped CVD graphene samples where higher temperature leads merely to a "redistribution of charge carriers within the valence or conduction band" [5] [4] [13]. Therefore, the carrier concentration does not increase significantly while the scattering rate is

Rhyan Foo Kune & James Heyman

enhanced by the increase in temperature. "As the lattice temperature increases, the phonon population increases resulting in a higher electron-phonon scattering rate" [5]. This is reflected through the adopted Drude model where the decrease in carrier mobility is the dominant term in the expression and leads to the observed decrease in conductivity after photo excitation.

$$\sigma_{Drude} = ne\mu$$

VI.   Conclusion

In our study, we introduce a novel technique to study the intrinsic dynamics of conducting films. Transient THz conductivity measurements and time-resolved measurements in the presence of a magnetic field allows us to independently determine the carrier density and effective scattering rate in thin conducting films, as well as the change of each quantity in photoconductive materials.

The experimental technique was applied to a p-type CVD graphene. The recorded complex conductivity agrees qualitatively with the established Drude response exhibiting a negative photoconductivity. Time-Resolved measurements indicate a transient induced THz transparency (decrease in conductivity) linked to an increase in the scattering rate (decrease in carrier mobility), consistent with previous studies. A model has been developed to fit our data using energy dependent electron-phonon scattering as described by Rana *et. al*. Using a Drude Model, which assumes a single effective scattering rate, to interpret our data, the results show that after photoexcitation, the effective scattering rate decreases by 7%, while the carrier population increases by only 2%, therefore leading to a net decrease in conductivity. Although consistent with some proposed models, our results do not correlate quantitatively with the predicted values. This is thought to be due to the strong dependence of graphene to the surrounding environment. [12]
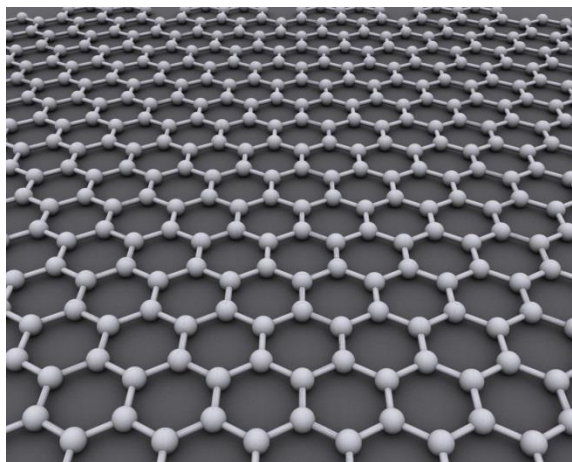
Acknowledgements

Figures

Figure 1: Molecular representation of graphene, a single-atom thick layer of carbon arranged in a honeycomb lattice. (http://en.wikipedia.org/wiki/Graphene)
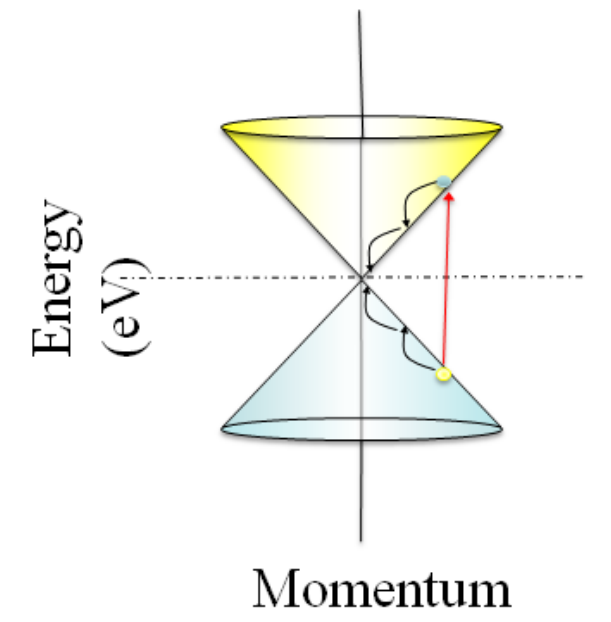
Figure 2: Graphene has a gapless band structure with linear energy dispersion describing "Dirac cones" around the Brillouin zone. At this point the valence and conduction band crosses.
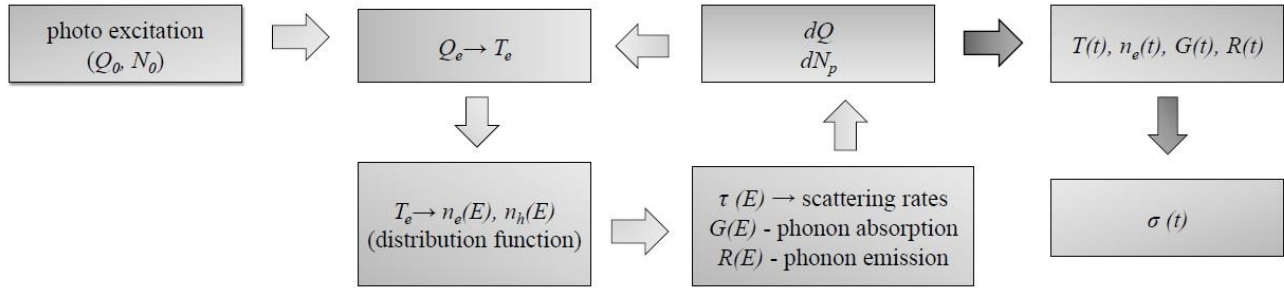
Figure 3: Model adapted from Rana *et al.* assuming a domination of carrier-phonon interaction in the scattering process. Photoexcitation gives an initial thermal energy Q_0 to the system which starts with an initial hole density N_0. The thermal energy is translated into a carrier temperature (T_e). The populations of electrons ($n_e(E)$) and holes ($n_h(E)$) are calculated assuming a single carrier temperature. The phonon emission and absorption rates were computed. We define the change in thermal energy, carrier distributions and phonon density from the phonon interactions. The previous steps are repeated to obtain T, $n_e(t)$, G and R as a function of time. The conductivity was obtained from the previous time evolution data to get $\sigma(t)$.
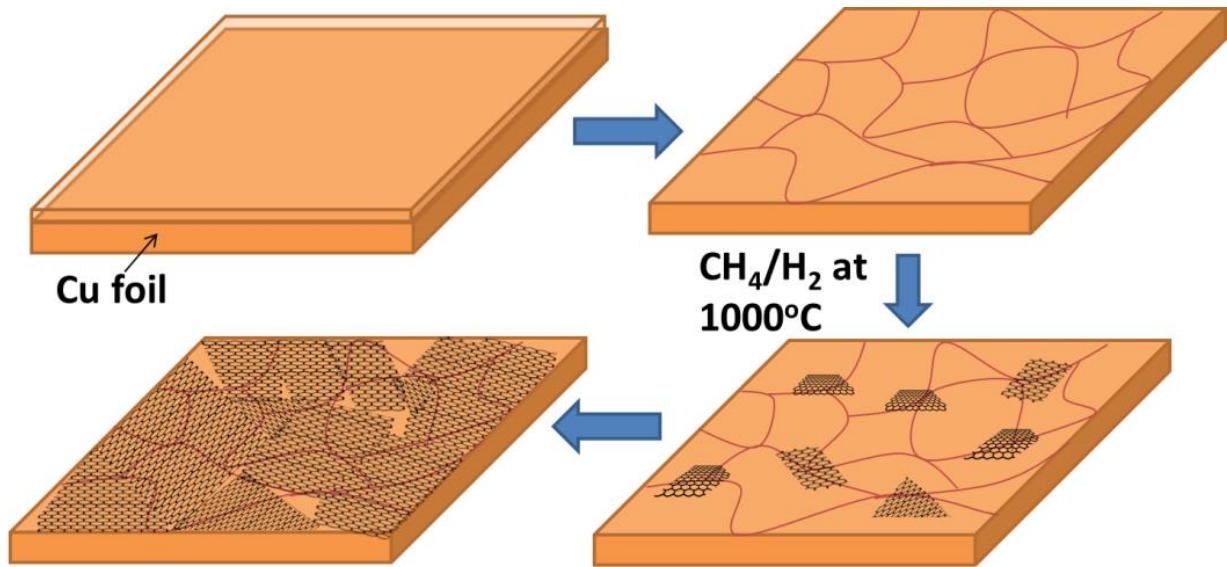
Figure 4: Chemical Vapor Deposition of graphene. In this process, a copper substrate is heated in a low vacuum furnace and a mixture of hydrogen and methane gas is injected into the chamber. Hydrogen causes the methane and copper to react, depositing a carbon atom onto the metal substrate. The metal is removed using an etchant solution and the graphene obtained is then transferred onto a sapphire substrate. [13]
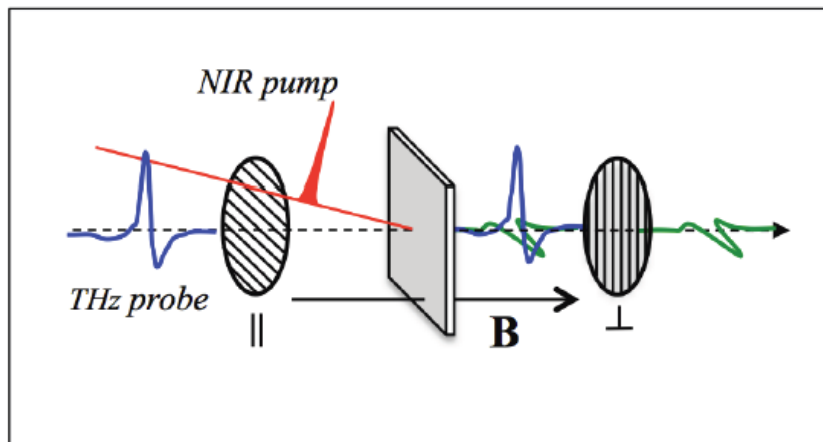
Rhyan Foo Kune & James Heyman

17

Figure 5: Geometry of the THz Faraday Rotation measurements. Linearly polarized THz pulses are incident to the sample. A magnetic field is applied and a second polarizer is used to analyze longitudinal or transverse signals. The sample is photo excited by a NIR pump pulse for time-resolved measurements. [14]
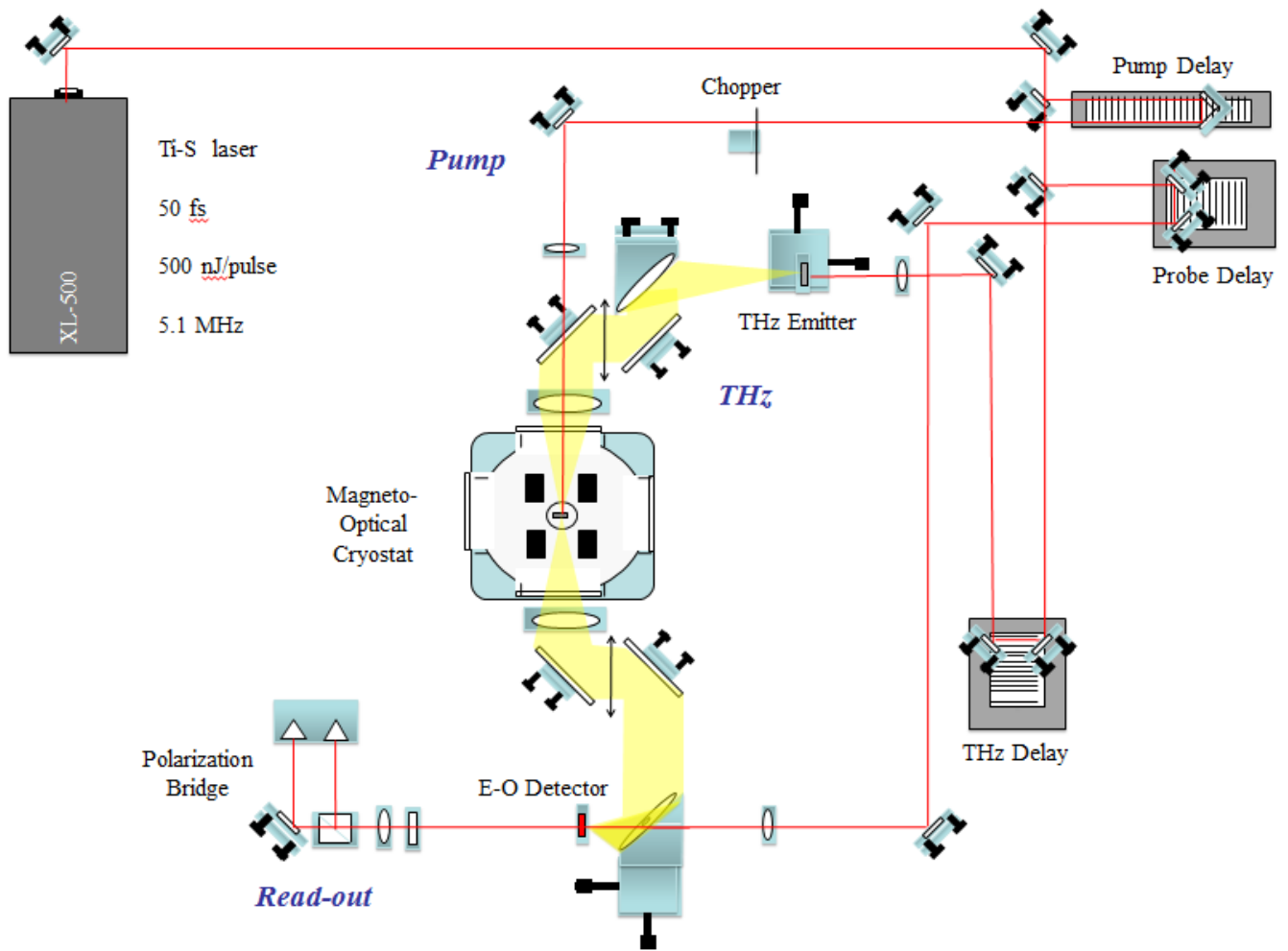
Figure 6: Experimental setup schema of a transient terahertz spectroscopy system. The laser beam is split into two beams. The first one is use as a pump beam to photoexcite the sample. The second beam is further split into one used to generate the THz pulse and the probe beam. The probe beam triggers the electro-optic detector.
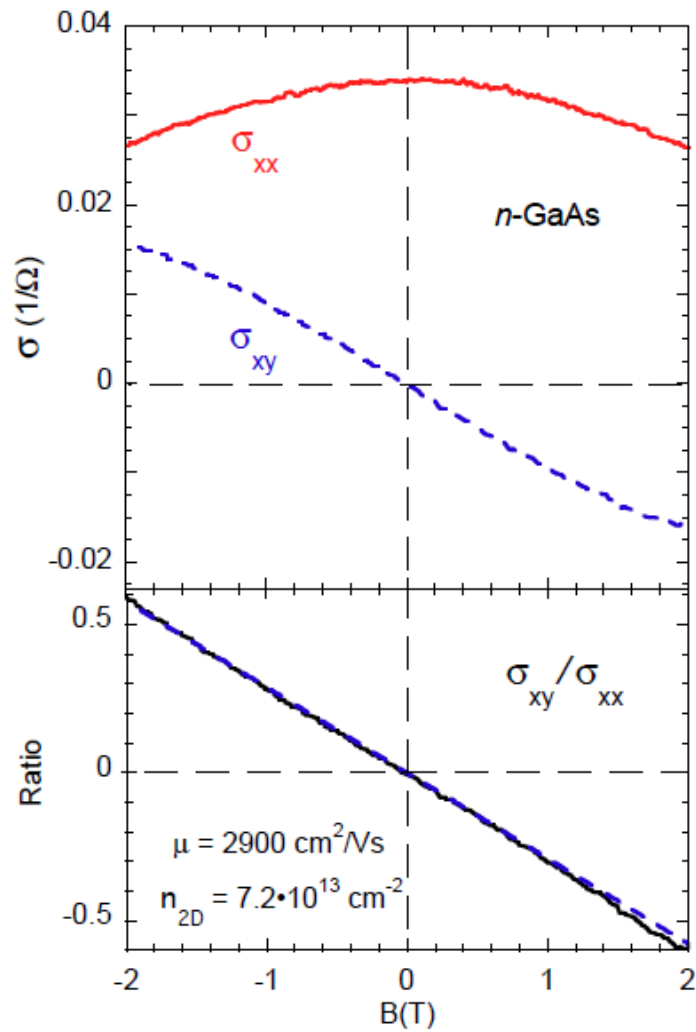
Figure 7: a) Longitudinal (σ_{xx}) and transverse (σ_{xy}) conductivity of an n-GaAs epitaxial layer versus magnetic field recorded through transient spectroscopy measurements. b) The ratio $\sigma_{xx}/\sigma_{xy}=\omega_c\tau=\mu B$ yielding the carrier mobility. [14]

Figure 8: a) Longitudinal (σ_{xx}) and transverse (σ_{xy}) conductivity of a p-type CVD graphene sample versus magnetic field recorded through transient spectroscopy measurements. b) The ratio $\sigma_{xx}/\sigma_{xy}=\omega_c\tau=\mu B$ yielding the carrier mobility. [14]
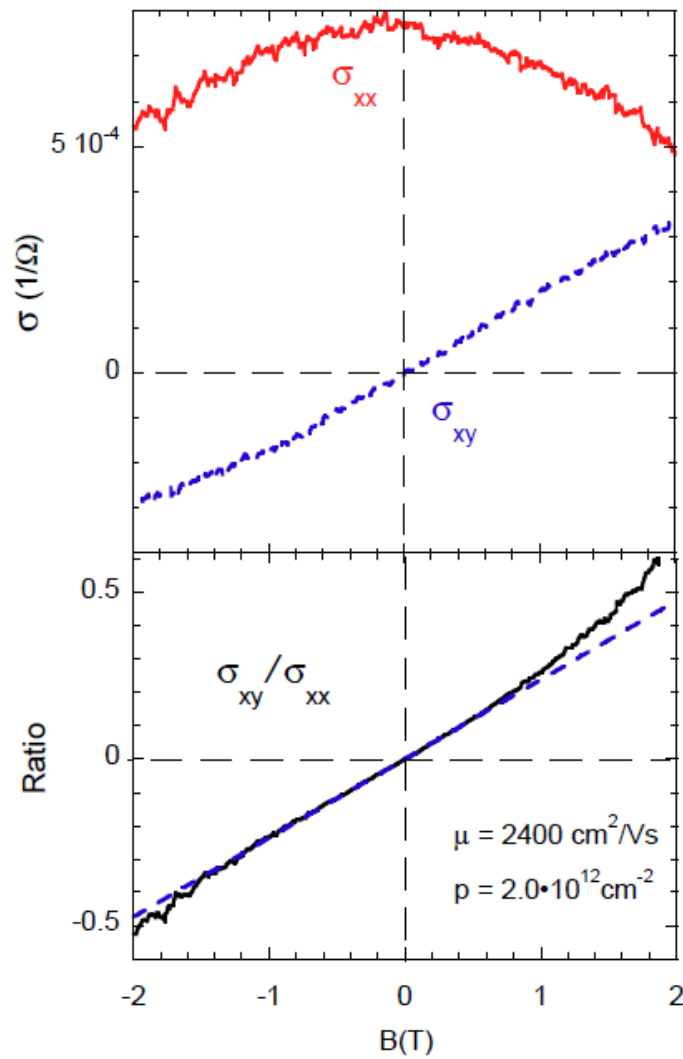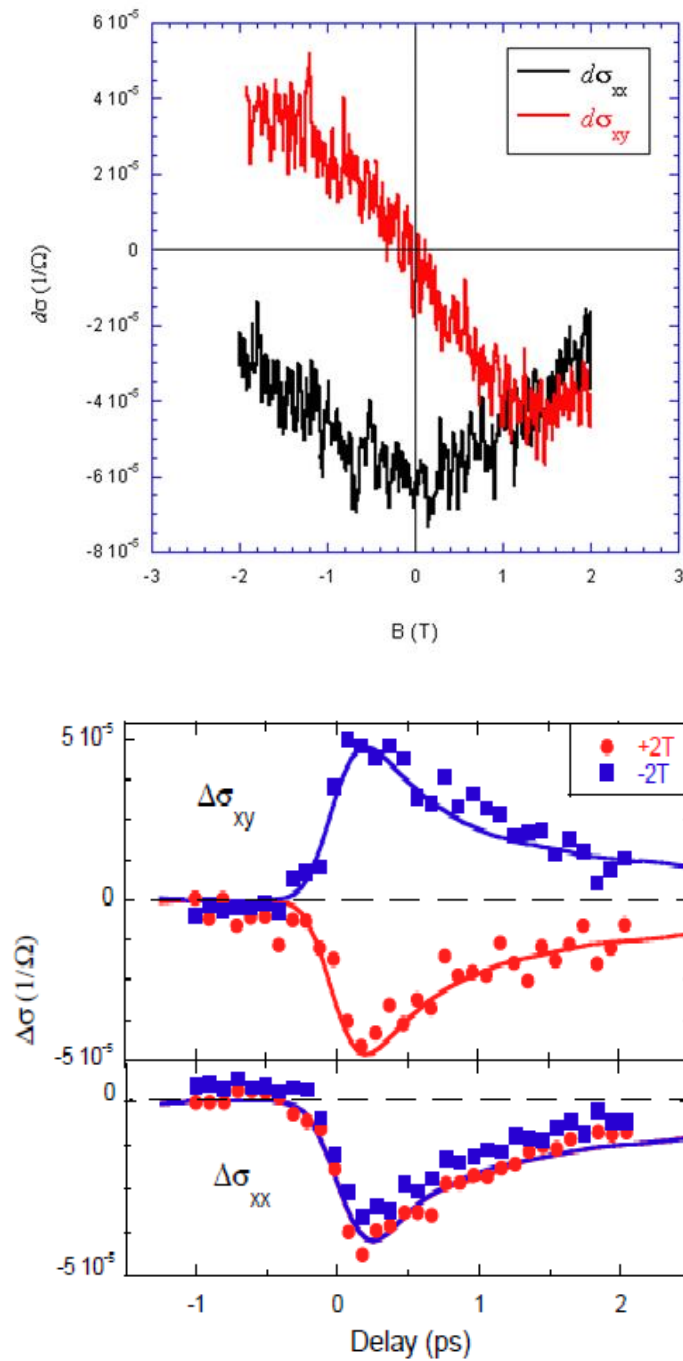
Figure 9: a) Longitudinal (dσ_{xx}) and transverse (dσ_{xy}) pump-induced change in conductivity of a p-type CVD graphene sample divided by the equilibrium longitudinal conductivity (σ_{xx}) versus magnetic field recorded through transient spectroscopy measurements. b) Fit to the time resolved measurements for a magnetic field of -2T and +2T. The model developed was adapted from Rana *et. al.*[8] [9]. [14]

Bibliography

1. *Measurement of ultrafast carrier dynamics in epitaxial graphene.* **Jahan M. Dawlaty, Shriram Shivaraman, Mvs Chandrashekhar, Farhan Rana, and Michael G. Spencer.** 2008, Applied Physics Letters 92.

2. *Ultrafast nonequilibrium carrier dynamics in a single graphene layer.* **M. Breusing, S. Kuehn, T. Winzer, E. Malic, F. Milde, N. Severin, J. P. Rabe, C. Ropers, A. Knorr, and T. Elsaesser.** 2011, Physical Review B 83.

3. *Optical spectroscopy of graphene: From the far infrared to the ultraviolet.* **Kin Fai Mak, Long Ju, Feng Wang, Tony F. Heinz.** 2012, Solid State Communications 152.

4. *Nonlinear THz Conductivity Dynamics in P-Type CVD-Grown Graphene.* **Harold Y. Hwang, Nathaniel C. Brandt, Hootan Farhat, Allen L. Hsu, Jing Kong, and Keith A. Nelson.** 2013, Physical Chemistry B 117.

5. *Controlling Graphene Ultrafast Hot Carrier Response from Metal-like to Semiconductor-like by Electrostatic Gating.* **S.-F. Shi, T.-T. Tang, B. Zeng, L. Ju, Q. Zhou, A. Zettl and F. Wang.** 2014, Nano Letters 14.

6. *Observation of a Transient Decrease in Terahertz Conductivity of Single-Layer Graphene Induced by Ultrafast Optical Excitation.* **Giriraj Jnawali, Yi Rao, Hugen Yan and Tony F. Heinz.** 2013, Nano Letters 13.

7. *Hole-channel conductivity in epitaxial graphene determined by terahertz optical-Hall effect and midinfrared ellipsometry.* **T. Hofmann, A. Boosalis, P. Kühne, C. M. Herzinger, J. A. Woollam, D. K. Gaskill, J. L. Tedesco and M. Schubert.** 2011, Applied Physics Letters 98.

8. *Carrier recombination and generation rates for intravalley and intervalley phonon scattering in graphene.* **Farhan Rana, Paul A. George, Jared H. Strait, Jahan Dawlaty, Shriram Shivaraman, Mvs Chandrashekhar, and Michael G. Spencer.** 2009, Physcal Review B 79.

9. —. **Farhan Rana, Paul A. George, Jared H. Strait, Jahan Dawlaty, Shriram Shivaraman, Mvs Chandrashekhar, and Michael G. Spencer.** 2009, Physical Review B 79.

10. *Large-Area Synthesis of High-Quality and Uniform Graphene Films on Copper Foils.* **Xuesong Li, Weiwei Cai, Jinho An, Seyoung Kim, Junghyo Nah, Dongxing Yang, Richard Piner, Aruna Velamakanni, Inhwa Jung, Emanuel Tutuc, Sanjay K. Banerjee, Luigi Colombo, and Rodney S. Ruoff.** 2009, Science 324.

11. *Electro-optic detection of THz radiation in LiTaO3, LiNbO3 and ZnTe.* **C. Winnewisser, P. Uhd Jepsen, M. Schall, V. Schyja, and H. Helm.** 1997, Applied physics letters 70.

12. *Extreme sensitivity of graphene photoconductivity to environmental gases.* **Callum J. Docherty, Cheng-Te Lin, Hannah J. Joyce, Robin J. Nicholas, Laura M. Herz, Lain-Jong Li, and Michael B. Johnston.** 2012, Nature Communications 3.

13. **Lee, Ajay Kumar and Chee Huei.** Synthesis and Biomedical Applications of Graphene: Present and Future Trends. *Advances in Graphene Science.* 2013.

14. *Ultrafast THz Faraday Rotation in Graphene.* **J. N. Heyman, R. F. Foo Kune, B. A. Alebachew, M. D. Nguyen, J.T. Robinson.** Accepted for publication, 2015, Journal for Applied Physics.

Rhyan Foo Kune & James Heyman

15. *Screening-induced temperature-dependent transport in two-dimensional graphene.* **E. H. Hwang, and S. Das Sarma.** 2009, Physical Review B 79.

16. *Ultrafast Optical-Pump Terahertz-Probe Spectroscopy of the Carrier Relaxation and Recombination Dynamics in Epitaxial Graphene.* **Paul A. George, Jared Strait, Jahan Dawlaty, Shriram Shivaraman, Mvs Chandrashekhar, Farhan Rana, and Michael G. Spencer.** 2008, Nano Letters 8.

17. *Ultrafast relaxation dynamics of hot optical phonons in graphene.* **Haining Wang, Jared H. Strait, Paul A. George, Shriram Shivaraman, Virgil B. Shields, Mvs Chandrashekhar, Jeonghyun Hwang, Farhan Rana, Michael G. Spencer, Carlos S. Ruiz-Vargas, and Jiwoong Park.** 2010, Applied Physics Letters 96.

18. *Review of Chemical Vapor Deposition of Graphene and Related Applications.* **Yi Zhang, Luyao Zhang, and Chongwu Zhou.** 2013, Accounts of chemical research 46.

19. *Terahertz and infrared transmission of an organic/inorganic hybrid thermoelectronic material.* **James Heyman, B. A. Alebachew, Z. S. Kaminski, M. D. Nguyen, N. E. Coates, and J. J. Urban.** 2014, Applied Physics Letters 104.

20. *Negative dynamic conductivity of graphene with optical pumping.* **V. Ryzhii, M. Ryzhii, and T. Otsuji.** 2007, Journal of Applied Physis 101.

21. *Ultrafast carrier dynamics and terahertz emission in optically pumped graphene at room temperature.* **S. Boubanga-Tombet, S. Chan, T. Watanabe, A. Satou, V. Ryzhii, and T. Otsuji.** 2012, Physical Review B 85.

22. *Graphene materials and devices for terahertz science and technology.* **Taiichi Otsuji, Stephane Albon Boubanga Tombet, Akira Satou, Hirokazu Fukidome, Maki Suemitsu, Eiichi Sano, Vyacheslav Popov, Maxim Ryzhii, and Victor Ryzhii.** 2012, MRS Bulletin 37.

23. *Ultrafast carrier dynamics in graphite.* **Markus Breusing, Claus Ropers, and Thomas Elsaesser.** 2009, Physical Review Letters 102.

24. *Graphene: Is It the Future for Semiconductors? An Overview of the Material, Devices, and Applications.* **Yaw Obeng, and Purushothaman Srinivasan.** 2011, The Electrochemical Society Interface.

Rhyan Foo Kune & James Heyman

24